The Astrophysical Journal Letters, 731:L3 (6pp), 2011 April 10 doi:10.1088/2041-8205/731/1/L3

INSIGHTS INTO FILAMENT ERUPTION ONSET FROM *SOLAR DYNAMICS OBSERVATORY* OBSERVATIONS

Alphonse C. Sterling[1,3], Ronald L. Moore[1], and Samuel L. Freeland[2]
[1] Space Science Office, VP62, NASA Marshall Space Flight Center, Huntsville, AL 35812, USA; alphonse.sterling@nasa.gov, ron.moore@nasa.gov
[2] Lockheed Martin Solar & Astrophysics Laboratory, Department/ADBS, B/252, 3251 Hanover Street, Palo Alto, CA 94304, USA
Received 2011 January 7; accepted 2011 February 3; published 2011 March 16

ABSTRACT

We examine the buildup to and onset of an active region filament confined eruption of 2010 May 12, using EUV imaging data from the *Solar Dynamics Observatory* (*SDO*) Atmospheric Imaging Array and line-of-sight magnetic data from the *SDO* Helioseismic and Magnetic Imager. Over the hour preceding eruption the filament undergoes a slow rise averaging ∼3 km s^{-1}, with a step-like trajectory. Accompanying a final rise step ∼20 minutes prior to eruption is a transient preflare brightening, occurring on loops rooted near the site where magnetic field had canceled over the previous 20 hr. Flow-type motions of the filament are relatively smooth with speeds ∼50 km s^{-1} prior to the preflare brightening and appear more helical, with speeds ∼50–100 km s^{-1}, after that brightening. After a final plateau in the filament's rise, its rapid eruption begins, and concurrently an outer shell "cocoon" of the filament material increases in emission in hot EUV lines, consistent with heating in a newly formed magnetic flux rope. The main flare brightenings start ∼5 minutes after eruption onset. The main flare arcade begins between the legs of an envelope-arcade loop that is nearly orthogonal to the filament, suggesting that the flare results from reconnection among the legs of that loop. This progress of events is broadly consistent with flux cancellation leading to formation of a helical flux rope that subsequently erupts due to onset of a magnetic instability and/or runaway tether cutting.

Key words: Sun: activity – Sun: filaments, prominences – Sun: flares – Sun: UV radiation

Online-only material: animations

1. INTRODUCTION

Filaments often undergo relatively slow rising motions from shortly before the onset of solar eruptions (e.g., Tandberg-Hanssen et al. 1980; Kahler et al. 1988; Chifor et al. 2007; Schmieder et al. 2008; Schrijver et al. 2008; Liewer et al. 2009; Cheng et al. 2010; Xu et al. 2010). We have been considering the implications of these early motions for the eruption trigger mechanism (Sterling & Moore 2003, 2004a, 2004b, 2005; Moore & Sterling 2006; Sterling et al. 2007a, 2007b, 2010). One general conclusion from our previous studies is that "tether-cutting" magnetic reconnection (e.g., Moore & LaBonte 1980; Moore & Roumeliotis 1992; Moore et al. 2001) occurs beneath the erupting filament in many eruptions, although it is difficult to determine whether this was the primary trigger for the eruption onset. With the launch of the *Solar Dynamics Observatory* (*SDO*), we can now reexamine this question with unprecedented wavelength coverage and spatial and temporal resolutions using the Atmospheric Imaging Array (AIA), along with high-quality magnetograms from the Helioseismic and Magnetic Imager (HMI). (Liu et al. 2010 present another *SDO* filament eruption).

Here we present early results from *SDO* for the onset of a filament eruption leading to a weak solar flare. The eruption "failed," in that it was "non-ejective" (Moore et al. 2001; Ji et al. 2003), without a coronal mass ejection (CME) being expelled. Nonetheless, the onset of the eruption should be virtually identical to that of many ejective eruptions. One feature we observe is a weak brightening prior to the start of the main flaring and rapid filament rise, as we have seen many times before in our previous studies, as have other workers, including Bumba & Kriviskỳ (1959), Martin (1980), Kai et al. (1983), van Hoven & Hurford (1984), Fárník et al. (2002), Chifor et al. (2007), Kim et al. (2007), and Liu et al. (2009). Our work here combined with previous studies shows that the processes producing preflare brightenings are important for preflare filament motions and for eruption onset for at least a class of solar eruptions, and by extension, CMEs (Harrison et al. 1985; Harrison 1986).

[3] Current address: JAXA/Institute of Space and Astronautical Science, Hinode Group, 3-1-1 Yoshinodai, Sagamihara, Kanagawa 229-8510, Japan.

2. DATA SET AND INSTRUMENTATION

NOAA records indicate that the event began in soft X-rays (SXRs) detected by the *GOES* 14 satellite on 2010 May 12 at 02:08 UT, reaching a peak at 02:22 UT and ending at 02:29 UT, producing a *GOES* B1.5 flare. It was observed with AIA (Title et al. 2006), and we extracted 400″ × 400″ "cutouts" of these data at wavelengths of 94, 131, 171, 193, 211, 304, and 335 Å, where the chief contributing ions and the primary temperature response can vary depending on the solar target being observed (O'Dwyer et al. 2010). We examined all wavelengths, but here focus on the 304 Å (with primarily contribution from He II, with peak log temperature response of 4.7 K), 171 Å (Fe IX, 5.85 K), and 193 Å (Fe XII, 6.2 K outside flaring regions) channels. The 171 Å and 193 Å images shared similar properties, and so we mainly present data from only the 193 Å and 304 Å channels here. The images have 0.″6 pixels and 12 s cadence. This eruption occurred in NOAA AR 11067, which was located at about N23W66 at eruption time. We also used HMI line-of-sight images of the region; we were not confident in using quantitative magnetic strength values due to the region's proximity to the limb, but use the images to observe qualitative changes of the field with time.

3. OBSERVATIONS

3.1. Filament Behavior in AIA Images

Figure 1 and the accompanying animations show the erupting filament in AIA 304 Å and 193 Å images. Spanning ∼40″,

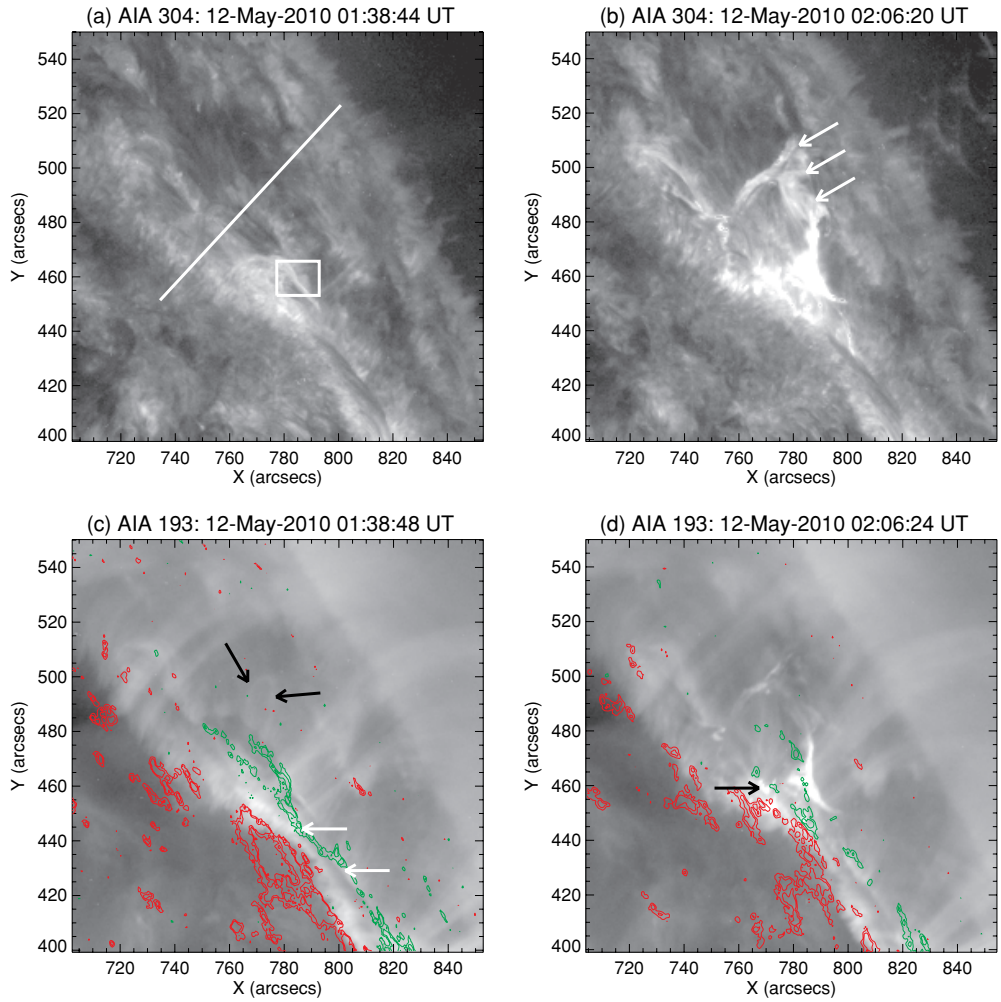

Figure 1. AIA images of the erupting filament in (a and b) the 304 Å and (c and d) the 193 Å channels. Panels (a) and (c) are at times when the preflare transient brightening is occurring near the SW end of the portion of the filament that erupts. Panels (b) and (d) are from when the main phase of the eruption is underway and the flare loops are brightening. In (a), the box shows the location of the preflare brightening, and the light curves in Figure 2 are from intensity integrated over this box. The fiducial line in (a) shows the path along which the filament trajectory is displayed in Figure 2. Arrows in (b) point to the filament, visible in emission at this time. The black arrow in (d) shows the location where the main flare arcade grows, which is between the legs of an arcade envelope loop of little shear shown by black arrows in (c). In (c) and (d), red and green contours are, respectively, positive and negative HMI magnetic polarities from (a) 2010 May 11 04:00:33 UT and (b) 2010 May 12 00:00:33 UT. White arrows in (c) point to locations on the magnetogram, the northern of which undergoes flux cancellation by the time of (d), while the field configuration at the southern location does not change much between (c) and (d). North is upward and west is to the right in these and all other solar images in this Letter.

(Animations [A, C] of this figure are available in the online journal.)

the erupting filament is only a portion of a filament complex that spans at least ∼150″. Figure 1(a) indicates with a box the location of the transient preflare brightening that occurs near the SW end of the portion of the filament that erupts. Around 01:40 UT the transient preflare brightening begins and is visible both in panels (a) and (c). Prior to ∼02:00 UT the filament is largely dark (absorbing) in all three channels (171 Å, 193 Å, and 304 Å), but with prominent flows apparent in the 304 Å channel. At ∼02:01 UT, the filament starts to show in emission, and the first flare ribbons become visible on the surface. By the time of panels (b) and (d), the eruption is underway and flare emission has started. The preflare brightening begins about 25 minutes prior to the main flare onset at 02:05 UT. The initial bright flare loops start at a location between the legs of a pre-eruption arcade envelope field of little shear (a field arching nearly orthogonal to the neutral line, Figures 1(c) and (d)).

Figure 2 shows the height of the filament as a function of time, measured using the 193 Å animation along the fiducial line of Figure 1(a), with corresponding velocity and light curves from the boxed region of Figure 1(a). There is slow rising motion of the filament, averaging ∼3 km s^{-1} between 01:00 UT and 01:55 UT; this is composed however of periods of near-zero-velocity "plateaus," such as at ∼01:30 UT and 01:50 UT, and periods of substantial upward velocities (∼10–20 km s^{-1}) such as at 01:10 UT and 01:45 UT. In addition, there is a substantial hump in the trajectory between ∼01:20 and 01:28 UT; this results from a very fine strand of the filament that reaches up and falls down along our fiducial line rather than the bodily behavior of the filament, but we retain it because it could be indicative of subtle but physically important filament motions. From around 01:40 UT, there is an unambiguous jump in the filament height that accompanies the preflare brightening apparent in all three light curves. This is followed by a period where the height is approximately constant, the last plateau for the filament before it erupts outward rapidly beginning about 02:00 UT.

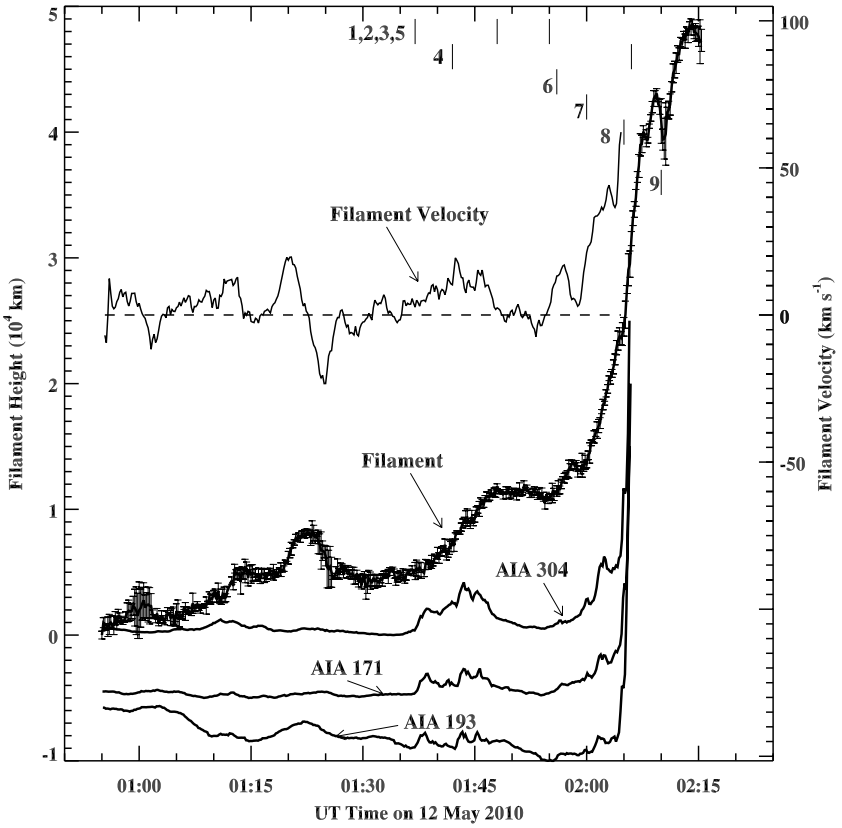

Figure 2. Trajectory labeled "filament" is height of the filament as a function of time, measured from 193 Å images along the fiducial line of Figure 1(a). Error bars are 1σ uncertainties obtained by three repeated measurements of the heights. The filament velocity is the derivative of the height curve smoothed over 10 pixels and 10 time steps (∼2 minutes), with the dashed line showing zero velocity. The three bottom plots are light curves for summed intensities over the box region of Figure 1(a) for AIA 304, 171, and 193 Å channels. Short vertical bars at the top of the figure show times of interest corresponding to events indicated in Table 1, with numbers to the left of the earliest bar of each horizontal row corresponding to the event numbers for the bars of that row.

Earlier upward filament movement between ∼01:05 and 01:15 UT is also accompanied by a series of brightenings weaker than that near 01:45 UT (for clarity we call these "weak brightenings" here, to distinguish from the preflare brightening near 01:45 UT); these weak brightenings are visible in the 304 Å animation, and some of the brightening spills into the region of the box of Figure 1(a), and therefore visible between ∼01:05 and 01:20 UT in the Figure 2 304 Å light curve, although the center of that earlier brightening is displaced somewhat from the Figure 1(a) box. As is clearly the case with the preflare brightening, the processes producing these weak brightenings may also induce a filament rise. It is difficult however to demonstrate a direct correlation in this data set because the earlier brightenings are weak and frequent over a short time span and because possible filament response to each appears comparable to the size of the error bars in the height profile.

Another feature of the erupting filament is helical-appearing motions (spinning or deformation into writhe) from near 01:40 UT, about coincident with the onset of the transient brightening. In the 304 Å animation, the filament appears to have no spinning motion prior to this time, while it has substantial spin (and/or helical deformation) afterward. In 193 Å it is less obvious whether the filament prior to 01:40 UT truly has no spin-like motion, but there is at least an increase in such motion from this time.

Starting from ∼01:56 UT, some portion of the filament transitions from absorption to emission in the hotter coronal lines, and concurrently from weaker emission to stronger emission at 304 Å. This is near the end of the last plateau phase of the filament, and the intensity enhancements accompany the rapid eruption beginning at about 02:00 UT. Even during this emission phase however, a portion of the erupting filament appears in absorption at least at 193 Å, where the images show the brighter material encasing the absorbing filament in a "cocoon" of emission.

Figure 3 shows in detail the flows and rotation of the filament, and the transition from absorption to emission of a portion of the filament. Prior to ∼01:40 UT we see persistent near-constant-velocity flows in 304 Å moving in two directions along the filament, but predominant from SW to NE. Using seven filament structural features in the 304 Å images to measure speeds, we find a value of 55 ± 10 km s^{-1} for the flow velocity between 01:13 UT and 01:35 UT. During the spinning phase we see moving emitting features in all three lines, but velocities are more difficult to measure reliably because the filament is moving upward while appearing to spin, the viewing perspective may be changing with time and with location along the length of the filament, and because the apparent spin rate may not be constant. With these cautions, we measured values during the post-01:40 UT phase between 50 and 100 km s^{-1}, based on the distance traveled in the plane in which we are viewing the filament (i.e., not accounting for the likely cylindrical shape of the apparently spinning structure). Table 1 summarizes our observed AIA morphological changes with this eruption.

3.2. Filament Behavior in HMI Line-of-sight Magnetograms

Magnetic cancellation often accompanies solar eruptions (e.g., Rust 1976; Wang & Shi 1993; Feynman & Martin

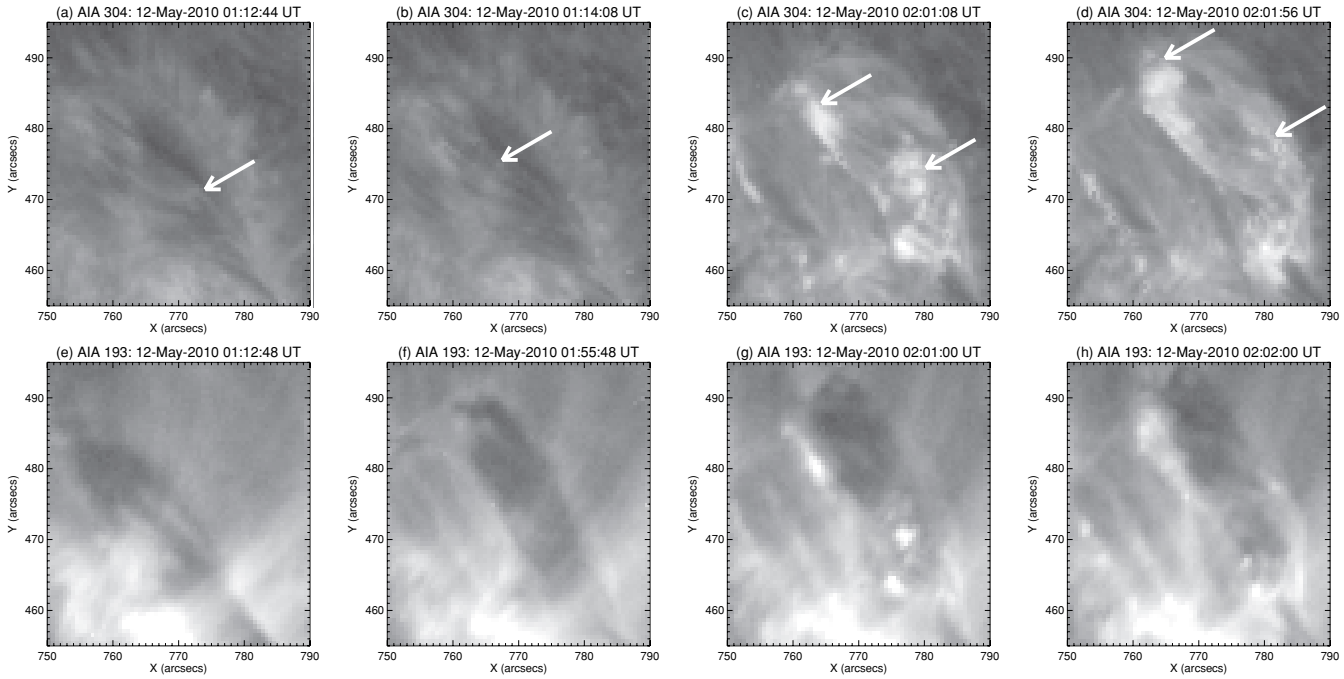

Figure 3. AIA images from the (a–d) 304 Å and (e–h) 193 Å channels, showing motions of the filament and the transition of a portion of the filament material from absorption to emission. Arrows in (a) and (b) track a moving feature (cf. Figure 1, animation C), suggesting velocities of ∼50 km s^{-1}. Similarly, arrows in (c) and (d) track rotating features as the filament appears to spin during eruption onset, with the velocities of those apparently rotating features (in the plane of the image) being ∼50–100 km s^{-1}. In 193 Å, the filament appears only in absorption in (e) and (f), but also in emission in (g) and (h).

Table 1
Progress of Events During Eruption

Period	Time (UT)	Observation
1	<00:55–∼01:37	Slow filament rise, some weak brightenings.
2	∼01:37–∼01:48	Transient preflare brightening near SW end of erupting filament.
3	”	Significant acceleration and upward rise of filament during time of preflare brightening.
4	∼01:42–∼02:06	Spin-like motions beginning at SW end of filament; initiate at location of preflare brightening.
5	∼01:48–∼01:55	Filament height stabilized.
6	From ∼01:56	Apparent flows over the filament; visible in 304 Å at least from <00:55 UT, but brightening in emission in 171 Å, 193 Å, and 304 Å from ∼01:56 UT.
7	From ∼02:00	Strong emissions starting below filament and onset of low-atmosphere ribbons, emission spreading to encompass absorbing filament material in a cocoon of emission that shows helical-appearing structure, and fast eruption begins.
8	∼02:05–∼02:25	Intense flare emissions in 193 Å (slightly different times in other channels) from location between feet of the low-shear envelope loop. Also strong brightenings from location of preflare brightening at SW end of filament.
9	From ∼02:10	Filament eruptive outward motion arrested; falls back to surface.

1995), and we examined line-of-sight magnetograms for this event. Due to a temporary limited availability of appropriate *SDO* full-disk data at the time of this writing, we used *Solar and Heliospheric Observatory* (*SOHO*)/Extreme ultra-violet Imaging Telescope and *SOHO*/Michelson Doppler Imager data to adjust the alignment of our AIA and HMI images, and as a result we only are confident in our resulting alignment to ∼10″ or so. Even with these conservative reservations, these data can tell us about the magnetic morphology for this eruption. Figures 1(c) and (d) show two magnetograms separated by 20 hr; there is cancellation of the field apparent at the location of the northern arrow between the two times. This cancellation is localized to a short region along the neutral line, with the locations of the southern arrow in Figure 1(c) still showing a separation between the red and green fields at the time of Figure 1(d). Moreover, because this separation at the southern arrow location persists, we are confident that the apparent cancellation we see at the northern arrow's location is real, and not an artifact resulting from the magnetogram's proximity to the limb.

This cancellation occurring some hours prior to eruption is a commonly observed phenomenon (e.g., Green et al. 2003; Nagashima et al. 2007; Sterling et al. 2007a, 2007b, 2010). The proximity of this cancellation to the location of the preflare transient brightening suggests that the transient brightening and the subsequent sequence of events result from the canceling field.

4. SUMMARY AND DISCUSSION

Our filament's buildup toward eruption shows several features that we and others have emphasized before (works cited in the introduction), such as a slow rise toward eruption; weak, pre-eruption brightenings in coronal emission corresponding closely with acceleration in the filament's rise trajectory; and

evidence for these preflare brightenings occurring at or near sites of magnetic flux cancellation (or emergence). The filament's preflare rise is unsteady, with periods of near-zero-velocity interspersed with short periods of acceleration, and we find evidence for onset or increase of helical spin or deformation of the filament at the time of the preflare brightening. There is also a suggestion that earlier weak brightenings may be correlated with smaller jumps in the filament height. Sterling et al. (2007a) found a correlation between preflare brightenings and inflections in the filament-rise profile, but in the case where the brightenings occurred away from the primary flaring core-field region. A feature we observe here that perhaps occurs in only a percentage of eruptions is that the main flare arcade begins between the legs of a low-shear envelope loop; this is consistent with the first bright flare loops resulting from reconnection among the legs of that low-shear loop, which differs markedly from the standard tether-cutting picture (Figure 1 of Moore et al. 2001) where initial flare-loop-producing reconnections are from among the most highly sheared core-field components.

The preflare brightening at ~01:45 UT is clearly followed by a substantial disruption of the filament, with resulting strong spinning or deformation of the filament. After stabilizing in height for $\lesssim$10 minutes, the filament begins its rapid eruption and also increases in emission, with the emission forming a helical structure that appears to be mainly confined to an outer surrounding cocoon shell of the filament and with a more central portion of the filament material seen in absorption wrapped inside. Then the main flare emissions start ~02:05 UT.

An implication of our observations is that the process producing the preflare brightening near 01:45 UT plays a key role in the onset of the eruption. The ultimate cause of this brightening is consistent with magnetic flux cancellation (Figures 1(c) and (d)) and broadly consistent with the idea of tether-cutting reconnection resulting in the eruption. In more detail however it is not clear why tether cutting would lead to the brightening of loops only *above* the filament that erupts, which appears to be the case in Figures 1(a) and 1(c); in at least the simplest view, tether cutting would be expected to result in brightening also *below* the filament that erupts (see Figure 1 of Moore et al. 2001). One possibility is that the canonical tether cutting is occurring beneath the filament, but the brightening in the lower product of this reconnection (the expected early sheared flare loops below the reconnection site) is too weak to be seen or is hidden from our view behind the absorbing filament. Another possibility is that, rather than as in the canonical tether-cutting picture, the brightening results from reconnection of nearly parallel field lines that cross over the top of the filament, similar to the idea suggested for the production of chromospheric penumbral jets and "type II" spicules via reconnection along tangential discontinuities of nearby fields (De Pontieu et al. 2007; Katsukawa et al. 2007). The weak brightenings over ~01:05–01:15 UT are below the filament, as expected by tether cutting. Likewise, the brightening in the cocoon-emission stage before and during onset of the fast eruption could be due to canonical tether cutting below the filament.

Many filaments undergo a period of enhanced "activation" prior to eruption (e.g., Kiepenheuer 1964; Rust 1976). In our case this may correspond to when the filament undergoes helical rotation or deformation after the main preflare brightening. This is followed by an increase in the filament's EUV intensity during eruption, which was also seen by Zarro et al. (1999), and similar brightening near eruption onset has also long been seen in chromospheric lines (Martin & Ramsey 1972). In addition, other workers (e.g., Williams et al. 2005, 2009; Liu et al. 2009) have also observed filaments displaying a helical structure during the initiation phase of eruption.

This event's behavior may be consistent with a class of theoretical and modeling work that argue for multiple stages to eruption. For example, Amari et al. (2010) find that a period of flux cancellation of the nature described by van Ballegooijen & Martens (1989; also see Moore & Roumeliotis 1992) transforms an arcade to a toroidal flux rope. Eventually this system becomes unstable, when the energy for outward eruption of the toroidal field flux rope exceeds the energy of the restraining field, where this restraining field's energy is largely determined by the photospheric fields as they continue to weaken due to the cancellation. For an example simulation run by Amari et al. (2010), this transformation period between the onset of cancellation and the eruption lasts 38 Alfvén travel times, τ_A. In our case, the erupting segment of the filament spans ~30,000 km. If we guess an Alfvén speed of 300 km s^{-1} for the active region filament field, then $\tau_A \sim 100$ s and $38\tau_A \sim 60$ minutes. From Figure 2 the time from the start of the transient brightenings until the eruption is about 20 minutes, and so the estimate from the Amari et al. (2010) example is long but not egregiously so, especially given our rough assumptions. Others (e.g., Fan & Gibson 2007; Aulanier et al. 2010) also discuss the onset of eruption due to the torus instability after a slower-rate buildup. This is also similar to several other loss-of-equilibrium eruption models (see Reeves et al. 2010, for a recent example, and references therein). In particular, the apparent helical structure during eruption could indicate onset of a kink instability (e.g., Török & Kliem 2005; Fan & Gibson 2007, and references therein).

We can summarize by saying our observations of this event are consistent with this scenario: gradual flux cancellation under the filament built the filament flux rope over time, causing it to rise gradually, while a few bursts of aborted runaway reconnection gave the steps in the slow rise along with the brightenings of the strands in and around the filament. Finally, due to MHD instability and/or runaway tether cutting, the growing filament flux rope began its fast eruption. As soon as it rose high enough, the legs (that were close to the neutral line due to photospheric flow) of the small-shear envelope field collapsed together under the rising filament flux rope, and runaway tether-cutting reconnection of these legs started making the main flare loops and further unleashed the eruption, until the eruption was squelched by the larger-scale overarching field of the active region.

We thank G. L. Slater for valuable assistance with the AIA data. *SDO* is a mission for NASA's Living With a Star (LWS) Program. A.C.S. and R.L.M. were supported by funding from NASA's Office of Space Science through the Solar Physics Supporting Research and Technology Program, the Sun–Earth Connection Guest Investigator Program, and the Living With a Star Targeted Research & Technology Program.

REFERENCES

Amari, T., Aly, J.-J., Mikíc, Z., & Linker, J. 2010, ApJ, 717, L26
Aulanier, G., Török, T., Démoulin, P., & DeLuca, E. E. 2010, ApJ, 708, 314
Bumba, V., & Kriviskỳ, L. 1959, Bull. Astron. Inst. Czech., 10, 221
Cheng, X., Ding, M. D., & Zhang, J. 2010, ApJ, 712, 1302
Chifor, C., Tripathi, D., Mason, H. E., & Dennis, B. R. 2007, A&A, 472, 967
De Pontieu, B., et al. 2007, PASJ, 59, S655
Fan, Y., & Gibson, S. E. 2007, ApJ, 668, 1232

Fárník, F., Hudson, H. S., Karlický, M., & Kosugi, T. 2002, A&A, 399, 1159
Feynman, J., & Martin, S. F. 1995, J. Geophys. Res., 100, 3355
Green, L. M., Démoulin, P., Mandrini, C. H., & van Driel-Gesztelyi, L. 2003, Sol. Phys., 215, 307
Harrison, R. A. 1986, A&A, 162, 283
Harrison, R. A., Waggett, P. W., Bentley, R. D., Phillips, K. J. H., Bruner, M., Dryer, M., & Simnett, G. M. 1985, Sol. Phys., 97, 387
Ji, H., Wang, H., Schmahl, E. J., Moon, Y.-J., & Jiang, Y. 2003, ApJ, 595, L135
Kahler, S. W., Moore, R. L., Kane, S. R., & Zirin, H. 1988, ApJ, 328, 824
Kai, K., Nakajima, H., & Kosugi, T. 1983, PASJ, 35, 285
Katsukawa, Y., et al. 2007, PASJ, 59, S577
Kiepenheuer, D. O. 1964, in The Physics of Solar Flares, ed. W. N. Hess (NASA SP-50; Washington, DC: NASA), 323
Kim, S., Moon, Y.-J., Kim, K.-H., Kim, Y.-H., Sakurai, T., Chae, J., & Kim, K.-S. 2007, PASJ, 59, 831
Liewer, P. C., et al. 2009, Sol. Phys., 256, 57
Liu, R., Liu, C., Wang, S., Deng, N., & Wang, H. 2010, ApJ, 725, L84
Liu, W., Wang, T.-J., Dennis, B. R., & Holman, G. D. 2009, ApJ, 698, 632
Martin, S. 1980, Sol. Phys., 68, 217
Martin, S. F., & Ramsey, H. E. 1972, in Solar Activity Observations and Predictions, ed. P. S. McIntosh & M. Dryer (Cambridge, MA: MIT Press), 371
Moore, R. L., & LaBonte, B. 1980, in Proc. IAU Symp. 91, Solar and Interplanetary Dynamics, ed. M. Dryer & E. Tandburg-Hanssen (Boston, MA: Reidel), 207
Moore, R. L., & Roumeliotis, G. 1992, in Eruptive Solar Flares, ed. Z. Svestka, B. V. Jackson, & M. E. Machado (Berlin: Springer), 69
Moore, R. L., & Sterling, A. C. 2006, in Solar Eruptions and Energetic Particles, ed. N. Gopalswamy, R. Mewaldt, & J. Torsti (Geophysical Monograph Series, Vol. 165; Washington, DC: AGU), 43
Moore, R. L., Sterling, A. C., Hudson, H. S., & Lemen, J. R. 2001, ApJ, 552, 833
Nagashima, K., Isobe, H., Yokoyama, T., Ishii, T. T., Okamoto, T. J., & Shibata, K. 2007, ApJ, 668, 533
O'Dwyer, B., Del Zanna, G., Mason, H. E., Weber, M. A., & Tripathi, D. 2010, A&A, 521, 21
Reeves, K. K., Linker, J. A., & Mikić Forbes, T. G. 2010, ApJ, 721, 1547
Rust, D. M. 1976, Sol. Phys., 47, 21
Schmieder, B., Bommier, V., Kitai, R., Matsumoto, T., Ishii, T. T., Hagino, M., Li, H., & Golub, L. 2008, Sol. Phys., 247, 321
Schrijver, C. J., Elmore, C., Kliem, B., Török, T., & Title, A. M. 2008, ApJ, 674, 586
Sterling, A. C., Chifor, C., Mason, H. E., Moore, R. L., & Young, P. R. 2010, A&A, 521, A49
Sterling, A. C., Harra, L. K., & Moore, R. L. 2007a, ApJ, 669, 1359
Sterling, A. C., & Moore, R. L. 2003, ApJ, 599, 1418
Sterling, A. C., & Moore, R. L. 2004a, ApJ, 602, 1024
Sterling, A. C., & Moore, R. L. 2004b, ApJ, 613, 1221
Sterling, A. C., & Moore, R. L. 2005, ApJ, 630, 1148
Sterling, A. C., et al. 2007b, PASJ, 59, S823
Tandberg-Hanssen, E., Martin, S. F., & Hansen, R. T. 1980, Sol. Phys., 65, 357
Title, A. M., Hoeksema, J. T., Schrijver, C. J., & The AIA Team 2006, COSPAR Plenary Meeting, 36th COSPAR Scientific Assembly, CD ROM 2600
Török, T., & Kliem, B. 2005, ApJ, 630, L97
van Ballegooijen, A. A., & Martens, P. C. H. 1989, ApJ, 343, 971
van Hoven, G., & Hurford, G. J. 1984, Adv. Space Res., 4, 95
Wang, J., & Shi, Z. 1993, Sol. Phys., 143, 119
Williams, D. R., Török, T., Démoulin, P., van Driel-Gesztelyi, L., & Kliem, B. 2005, ApJ, 628, L163
Williams, D. R., et al. 2009, PASJ, 61, 493
Xu, Y., Jing, J., & Wang, H. 2010, Sol. Phys., 264, 81
Zarro, D. M., Sterling, A. C., Thompson, B. J., Hudson, H. S., & Nitta, N. 1999, ApJ, 520, L139